The Plant Cell, Vol. 24: 5159–5176, December 2012, www.plantcell.org

In Planta Stage-Specific Fungal Gene Profiling Elucidates the Molecular Strategies of *Fusarium graminearum* Growing inside Wheat Coleoptiles[W][OA]

Xiao-Wei Zhang,[a,b,1] Lei-Jie Jia,[a,b,1] Yan Zhang,[a,b] Gang Jiang,[a,b] Xuan Li,[c] Dong Zhang,[a] and Wei-Hua Tang[a,2]

[a] National Key Laboratory of Plant Molecular Genetics, Institute of Plant Physiology and Ecology, Shanghai Institutes for Biological Sciences, Chinese Academy of Sciences, Shanghai 200032, China

[b] Graduate School of Chinese Academy of Sciences, Institute of Plant Physiology and Ecology, Shanghai 200032, China

[c] Key Laboratory of Synthetic Biology, Institute of Plant Physiology and Ecology, Shanghai Institutes for Biological Sciences, Chinese Academy of Sciences, Shanghai 200032, China

The ascomycete *Fusarium graminearum* is a destructive fungal pathogen of wheat (*Triticum aestivum*). To better understand how this pathogen proliferates within the host plant, we tracked pathogen growth inside wheat coleoptiles and then examined pathogen gene expression inside wheat coleoptiles at 16, 40, and 64 h after inoculation (HAI) using laser capture microdissection and microarray analysis. We identified 344 genes that were preferentially expressed during invasive growth in planta. Gene expression profiles for 134 putative plant cell wall–degrading enzyme genes suggest that there was limited cell wall degradation at 16 HAI and extensive degradation at 64 HAI. Expression profiles for genes encoding reactive oxygen species (ROS)–related enzymes suggest that *F. graminearum* primarily scavenges extracellular ROS before a later burst of extracellular ROS is produced by *F. graminearum* enzymes. Expression patterns of genes involved in primary metabolic pathways suggest that *F. graminearum* relies on the glyoxylate cycle at an early stage of plant infection. A secondary metabolite biosynthesis gene cluster was specifically induced at 64 HAI and was required for virulence. Our results indicate that *F. graminearum* initiates infection of coleoptiles using covert penetration strategies and switches to overt cellular destruction of tissues at an advanced stage of infection.

INTRODUCTION

Fusarium graminearum (sexual state *Gibberella zeae*) is a fungal pathogen capable of causing head blight and seedling blight in wheat (*Triticum aestivum*) and other cereals (Cook 1968; Dal Bello et al., 2002; O'Donnell et al., 2004; Asran and Eraky Amal, 2011). The infection starts when *F. graminearum* spores (asexual conidia or sexually derived ascospores) land on the surface of host plant tissues, such as florets or seedlings. *F. graminearum* spores germinate to form germ tubes, and the germ tubes further extend and develop into hyphae. Hyphae can directly penetrate some surfaces within florets (Boenisch and Schäfer, 2011) or enter plant tissues through natural openings (Bushnell et al., 2003) or wounds produced by hail or insects (Reid et al., 1994). Once inside the host plant, *F. graminearum* grows inter- and/or intracellularly, mainly in hyphal form, prior to sporulation (Jansen et al., 2005; Rittenour and Harris, 2010). Host plants progressively develop disease symptoms in pace with *F. graminearum* hyphal growth in planta.

Extensive molecular and genetic studies have revealed that the deoxynivalenol (DON) biosynthesis pathway and mitogen-activated protein kinase signaling cascades are important for *F. graminearum* pathogenesis (Walter et al., 2010; Kazan et al., 2012). DON, a trichothecene mycotoxin that can inhibit protein synthesis (Rocha et al., 2005), is produced by *F. graminearum* during head blight infection and is required for the spreading of pathogen throughout the rachis (Jansen et al., 2005). Several lytic enzymes and numerous other proteins involved in iron uptake, sterol trafficking, nitrate transport, and reactive oxygen species (ROS) production have also been linked to pathogenesis (reviewed in Walter et al., 2010). Recently 42 protein kinase genes and 62 transcription factor genes were found to be required for wheat head infection (Son et al., 2011; Wang et al., 2011). However, these studies have not provided a complete blueprint for pathogenesis.

The availability of an annotated complete genome (Cuomo et al., 2007; Ma et al., 2010; Wong et al., 2011) and a whole-genome oligonucleotide microarray (Güldener et al., 2006) allows robust profiling of *F. graminearum* gene expression, which could provide important biological insights. Because diseases are developed in conjunction with pathogen growth in planta, delineating fungal gene expression on a genome-wide scale during discrete stages of infection should provide new insights into pathogenesis from a global viewpoint that were not obtained from previous studies. For example, although it is evident from previous research that *F. graminearum* should produce plant cell wall–degrading enzymes (CWDEs) as part of the

[1] These authors contributed equally to this work.

[2] Address correspondence to whtang@sibs.ac.cn.

The author responsible for distribution of materials integral to the findings presented in this article in accordance with the policy described in the Instructions for Authors (www.plantcell.org) is: Wei-Hua Tang (whtang@sibs.ac.cn).

[W] Online version contains Web-only data.

[OA] Open Access articles can be viewed online without a subscription.

www.plantcell.org/cgi/doi/10.1105/tpc.112.105957

infection strategy, and more than 70 CWDE genes were found to be expressed during *F. graminearum* infection of plants or incubation with plant extracts (Walter et al., 2010), we still don't understand the timing and sequential relationship of CWDE production that occurs in conjunction with *F. graminearum* in planta growth. We also don't know whether or when *F. graminearum* produces toxic secondary metabolites, other than DON, that compromise the host. Finally, pathogens must establish nutrient acquisition from the host (Divon and Fluhr, 2007), but we have few insights into the metabolic adjustments that allow *F. graminearum* to grow in planta.

Furthermore, *F. graminearum* is a facultative pathogen that can readily grow in culture and inside its host. The morphological changes that occur during growth, including spore germination, germ tube extension, and hyphal growth, are roughly similar during in vitro and in planta growth (Trail, 2009). With carefully controlled cultivation conditions that synchronize fungal growth, gene expression profiles of *F. graminearum* grown in vitro have been reported for four time points (0, 2, 8, and 24 h) (Seong et al., 2008). Indeed, elucidating differences in fungal gene expression patterns between in planta– and in vitro–grown *F. graminearum* during different developmental stages should be valuable for differentiating pathogenesis-relevant events from events that are essential for fungal growth rather than pathogenesis.

Several in planta profiling studies using bulk infected tissues have led to the identification of many genes expressed during infection (Güldener et al., 2006; Stephens et al., 2008; Lysøe et al., 2011). However, these studies suffered from significant noise from plant tissues and a lack of control over the developmental stages of the sampled fungi; therefore, changes in in planta fungal gene expression could not be monitored. For example, *F. graminearum* gene profiling during floret infection of wheat and barley (*Hordeum vulgare*) both indicated that the number of fungal genes expressed during infection increased over time, within 24 to 96 h after inoculation (HAI) (Güldener et al., 2006; Lysøe et al., 2011), but it can't be excluded that this increase was caused by the increase in fungal biomass that accompanies fungal proliferation inside the host. In addition, profiling at an early time point in infection (such as 24 HAI) revealed a significantly smaller number of expressed genes than profiling at any time point revealed for in vitro growth. This significant difference in profiling depth hindered the genome-wide comparison of gene expression data between in planta– and in vitro–grown pathogen.

Laser microdissection (LM) provides a means to separate the bulk of host tissue from the pathogen prior to expression profiling, thus greatly increasing the signal-to-noise ratio (Tang et al., 2012). Combined with the use of transgenic fungal strains that constitutively express fluorescent proteins in the fungal cytosol to visualize fungal infection, LM has been successfully applied to in planta profiling of the maize (*Zea mays*) anthracnose stalk rot fungus *Colletotrichum graminicola* at a single infection stage called "breakout," enabling the identification of 437 fungal genes that are upregulated in planta (Tang et al., 2006). In this work, using similar methods and carefully synchronizing in planta fungal growth, we analyzed the global gene expression profiles of *F. graminearum* hyphae growing inside wheat coleoptiles at three distinct stages of infection and subsequently compared these data to in vitro profiling data. Our results document a number of stage-specific gene expression patterns that can be ascribed to five distinct metabolic strategies: (1) stage-dependent deployment of CWDEs, (2) early production of specific cell surface-interacting proteins, (3) early mitigation and later production of ROS, (4) a shift in energy metabolism toward glyoxalate use, and (5) later onset of potentially phytotoxic secondary metabolite production. We were further able to validate the roles of several individual genes in these pathways in pathogenesis using targeted gene disruption and a quantitative bioassay for virulence.

RESULTS

F. graminearum Hyphae inside Coleoptiles at 16, 40, and 64 HAI Represent Three Distinct Stages of in Planta Growth

We set out to chart the dynamics of global gene expression in *F. graminearum* that occurs in conjunction with growth inside the host plant. Using the strain AmCyanPH-1, which constitutively expresses AmCyan fluorescent protein without affecting fungal growth (Yuan et al., 2008), we can track *F. graminearum* growth inside the host plant. *F. graminearum* typically causes head blight due to the infection of florets. However, it is difficult to synchronize *F. graminearum* growth in florets, as florets possess diverse surface features and distinct structures (caryopses, paleas, lemmas, and glumes) with defense mechanisms that might differ in subtle or major ways. The coleoptile, the outermost layer of the seedling shoot, comprises nearly identical cells and is among the tissues infected by *F. graminearum* when seedling blight occurs. We sprayed spore suspensions of *F. graminearum* strain AmCyanPH-1 on intact coleoptiles of 2-d-old wheat seedlings. Most of the coleoptiles split naturally within 1 to 2 d after inoculation (DAI), and *F. graminearum* hyphae could be observed inside coleoptile cells within 3 to 7 DAI (see Supplemental Figure 1 online), with dark-brown lesions becoming apparent on the coleoptiles of inoculated seedlings 10 to 14 DAI. Lesion progression speed and size varied among seedlings.

To synchronize infection beyond what could be achieved by spray inoculation, we inoculated wounded coleoptiles with a spore suspension. The appearance of symptoms often progressed in a similar manner among infected seedlings (Figure 1A; see Supplemental Figure 2 online). Within 24 HAI, small brown lesions at the tops of infected coleoptiles were first visible and continued to expand. After 7 to 10 DAI, the lesions reach ~1 cm in length (Figure 1A). Using fluorescence microscopy, we observed a large number of *F. graminearum* spores that germinated on the coleoptile surface by 10 HAI. By 12 HAI, more germ tubes emerged and grew toward the wounds or openings of stomata (Figure 1B). From 16 to 64 HAI, invasive hyphae that entered through wounds quickly elongated inside the coleoptiles, but those that entered through the stomata were often isolated inside the cavity underneath the stomata by 72 HAI (Figure 1B; see Supplemental Figure 3 online). From 72 to 160 HAI, *F. graminearum* continued to grow inside the host, mainly in

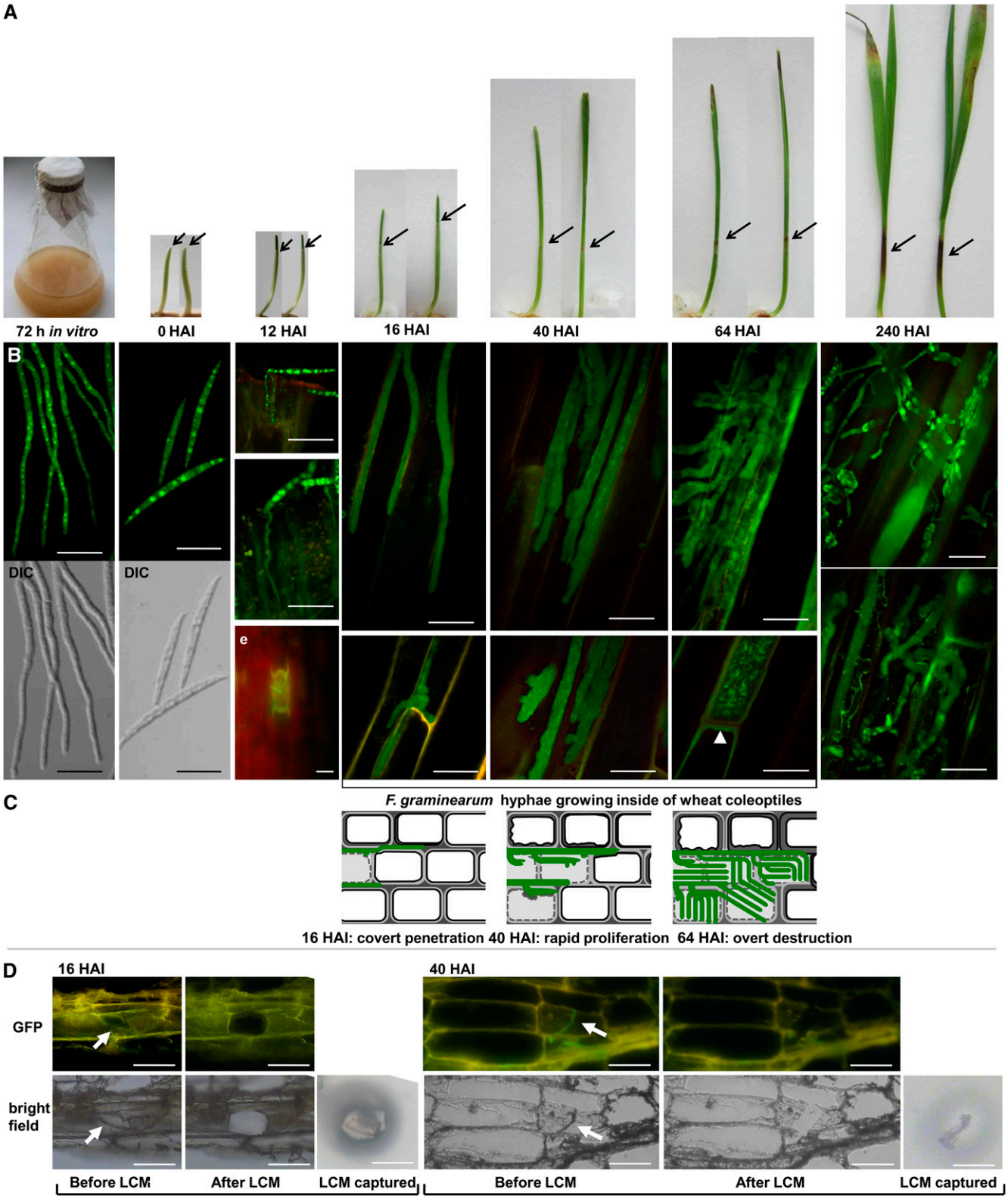

Figure 1. *F. graminearum* Proliferation in Vitro and inside Wheat Coleoptiles.

hyphal form. At 170 to 240 HAI, abundant fungal growth became visible on the surface of the lesions, and some were sporulating (Figure 1B). The sporulation stage is considered to be the end stage of an infection cycle (Divon and Fluhr, 2007).

The 16 HAI time point is the earliest time point at which uniform hyphal growth occurs inside live host tissues; before 16 HAI, we mainly observed germ tubes migrating at the wounding sites. From 16 to 64 HAI, hyphae that entered through wounds had a similar appearance. With more careful observation, we found that the hyphae inside the host displayed some different growth path preferences and morphological features at different time points within 16 to 64 HAI. At 16 to 20 HAI, the fungal hyphal frontier extended out from the cutting site to the neighboring plant cells; usually only one hypha was visible per invaded plant cell, and the hyphae often grew intercellularly or elongated longitudinally along the cell wall (Figure 1B; see Supplemental Figure 2 online). The hyphal tips rarely branched, and the hyphal width was ~4 μm. At 24 to 40 HAI, invasive hyphae grew more intracellularly and aggressively, and multiple (two to five) hyphae were usually visible per invaded plant cell. The hyphal frontier usually moved further forward into fresh coleoptile tissue (~500 μm away from cutting edge), and the invasive hyphae often had branched tips (Figure 1B; see Supplemental Figure 2 online); some hyphae grew in parallel. These hyphae often contained large vacuoles in their cytosol and were ~6 μm wide, wider than those observed at 16 HAI (see Supplemental Figure 2 online). At 60 to 70 HAI, roughly 60% of the penetrating hyphae filled the invaded plant cells, while 40% were still entering neighboring plant cells (see Supplemental Figure 2 online). The cytosol-expressed AmCyan fluorescence of the hyphae at this stage was often aggregate, unlike the uniform cytosolic distribution observed at 16 and 40 HAI (Figure 1B). Based on these distinct features (Figure 1C), we conclude that hyphae inside the coleoptile at 16, 40, and 64 HAI represent three distinct stages of in planta growth after the pathogen enters the plant through wounds.

The in Planta– and in Vitro–Grown *F. graminearum* Transcriptomes Are Similar in Size but Have Very Different Features

We used LM to isolate homogenous population of *F. graminearum* hyphae inside the coleoptile at 16, 40, and 64 HAI (Figure 1D), carefully avoiding the distinct fungal structures underneath the stomata and epiphytic hyphae spreading over the coleoptile surface at all capture time points. Samples of the conidia used for inoculation (0 HAI) were collected to represent the initial time point, and infected tissues at 240 HAI were also collected to represent the end stage of the infection cycle. RNA derived from these samples was hybridized to the *F. graminearum* Affymetrix GeneChip (Güldener et al., 2006). Results of our microarray analysis derived from laser-captured samples showed that 5684 (42%), 4215 (31%), and 5007 (37%) genes were expressed at 16, 40, and 64 HAI, respectively (see Supplemental Figure 4 online). This indicates that, after eliminating the interference caused by the increased fungal biomass that accompanies fungal proliferation, the number of fungal genes expressed during infection did not increase with post-inoculation time (during the 16 to 64 HAI period).

Seong et al. (2008) found that ~5000 to 6000 genes were expressed at the 0-, 2-, 8-, and 24-h time points, which represent the in vitro growth stages, including spore, spore swelling, early hyphal growth, and hyphal growth with branching, respectively. We performed microarray analysis of *F. graminearum* grown in vitro at the 72-h time point (in which hyphal growth was similar to that at 24 h) and detected 5746 (43%) genes that were expressed (see Supplemental Figure 4 online). These results show that the total number of genes expressed in planta at an individual stage was similar to that of conidia and hyphae grown in vitro.

The comparably deep gene profile that we obtained allowed us to perform a transcriptomic comparison of *F. graminearum* grown in planta versus in vitro within a similar time frame after global normalization. From a global viewpoint, combined principal component analysis (Figure 2A) shows that the transcriptomes of hyphae grown in planta (16, 40, 64, and 240 HAI) were more similar to each other than to transcriptomes of hyphae grown in vitro (2, 8, 24, and 72 h) or to the transcriptomes of spores (0 HAI and 0 h). These results were expected, given the difference in growth environments in vitro and in planta and the differences in morphology between spores and hyphae. These results also demonstrate that, although we employed different methods from those of Seong et al. (2008), the overall similarity of the transcriptome reflects the nature of fungal behavior rather than the method of sample preparation.

Using in planta and in vitro expression data, we identified 344 genes that were more strongly expressed during the in planta growth stages (during at least one stage among 16, 40, and 64 HAI) than at any in vitro growth stages (including 0, 2, 8, 24, and 72 h in the medium and spore suspension stage). These genes were therefore designated in planta preferential genes (see Supplemental Data Set 1 online). This set of genes likely includes genes that encode proteins that are of particular importance to fungal proliferation in coleoptiles. Enrichment analysis

Figure 1. (continued).

(A) *F. graminearum* AmCyanPH-1 grown in vitro (72 h) and in wheat seedlings before and after inoculation with *F. graminearum* AmCyanPH-1 at the indicated time points. Arrows point to lesions caused by *F. graminearum* infection. HAI, hours after inoculation.

(B) Representative microscopy images of *F. graminearum* AmCyanPH-1 at the time points listed above the figure. The arrowhead points to plant cell wall deposition. DIC, differential interference contrast; e, epifluorescence. Bar = 20 μm.

(C) Diagrams of the three stages of *F. graminearum* proliferation inside wheat coleoptiles. Green lines represent fungal hyphae.

(D) Representative pictures of laser capture microdissection of *F. graminearum* hyphae growing inside wheat coleoptiles at 16 and 40 HAI. White arrows point to hyphae. Bar = 50 μm.

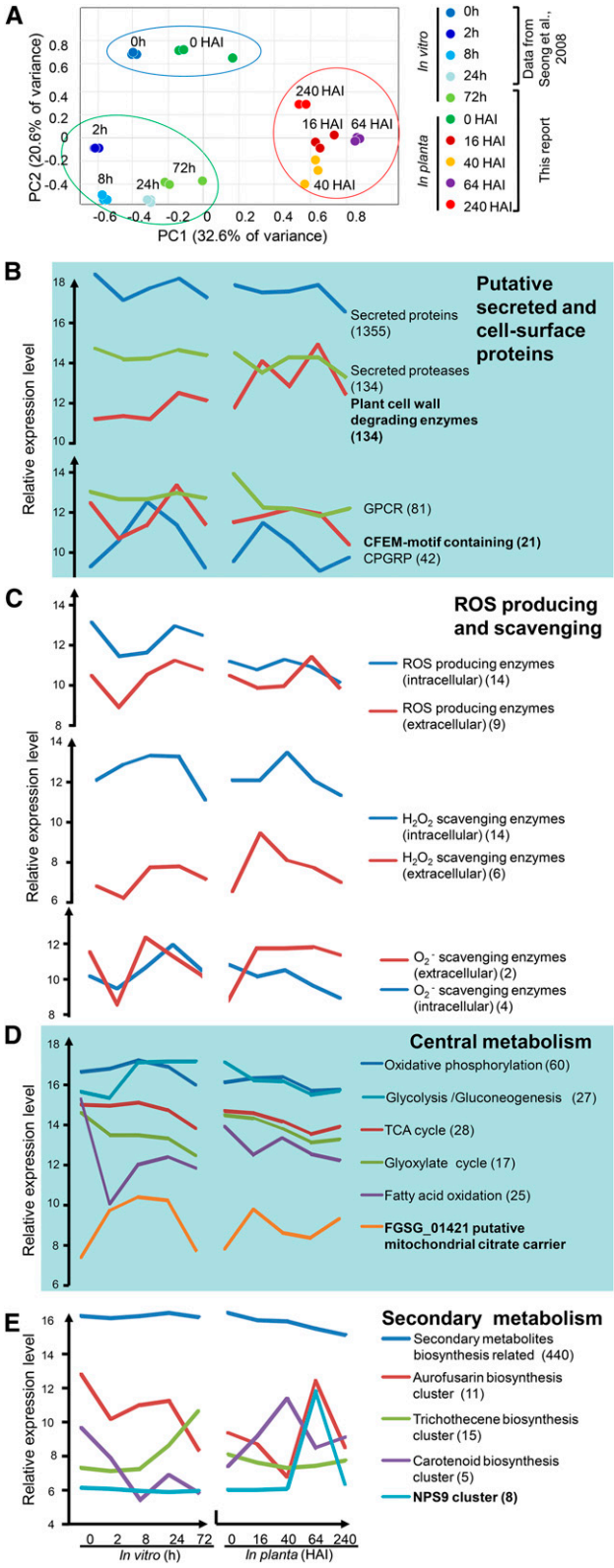

Figure 2. Global Expression Analysis Shows Distinct Patterns of Gene Expression in *F. graminearum* Growing inside Wheat Coleoptiles Compared with in Vitro–Grown Fungus.

of predicted subcellular compartmentation categories showed that, of the 344 such genes, 141 (41%) encode putative secreted proteins (compared with 1355 genes that encode putative secreted proteins overall [i.e., ~10% of the 13,427 *F. graminearum* unigenes included in this study]). This enrichment analysis result is not surprising, given that the secreted proteins produced by the pathogen during in planta proliferation are at the forefront of interaction with the host. The total expression of the 1355 putative secreted proteins was similar to that of spores or in vitro–grown hyphae (Figure 2B), but the number of expressed putative secreted protein genes at 16 or 64 HAI was ~30 to 40% greater than that at any other stage that was examined (see Supplemental Data Set 2 online), supporting the notion that the in planta secretome is more diverse than the in vitro secretome.

Enrichment analysis of the FunCat (Ruepp et al., 2004) gene families (see Supplemental Data Set 3 online) shows that several different types of genes, including genes that encode putative extracellular cell wall degradation-related compounds (such as compounds involved in carbohydrate metabolism, extracellular polysaccharide degradation, and degradation/modification of exogenous compounds), genes related to nutrition acquisition (such as genes involved in cellular import, carbon compound, and carbohydrate transport), genes related to secondary metabolism, and disease and virulence- and defense-related genes, were significantly enriched in the in planta preferentially expressed group of genes, while genes required for fungal growth and development (such as genes related to the cell cycle, DNA processing, and transcription) were significantly depleted in this group.

Based on these results, along with our current understanding of pathogenesis-related events, we selected the following functional categories for detailed analysis, including expression analysis of multiple time points both in planta and in vitro: secreted or plasma membrane–localized proteins, including plant CWDEs and other putative cell surface proteins; ROS producing and scavenging proteins; and proteins involved in central metabolic pathways and secondary metabolism.

Expression Profiles of Plant CWDEs Suggest That Fungal Hyphae First Penetrate and Later More Extensively Digest Cell Walls

Among the secretome genes, the most significantly upregulated group was the putative CWDEs. Although *F. graminearum* is assumed to produce many PCWDEs as a part of an infection strategy, our data open up the possibility that the expression of various PCWDEs can be delineated as the infection process progresses. The aggregate expression levels of 134 verified or

(A) Principal component analysis of the transcriptomes during in vitro and in planta growth. HAI, hours after inoculation.
(B) to **(E)** Expression trends of genes encoding proteins in four functional categories: putative secreted and cell surface proteins **(B)**, ROS-producing and scavenging **(C)**, central metabolic pathways **(D)**, and secondary metabolism **(E)**. *y* axes are $\log_2$-transformed total intensities.

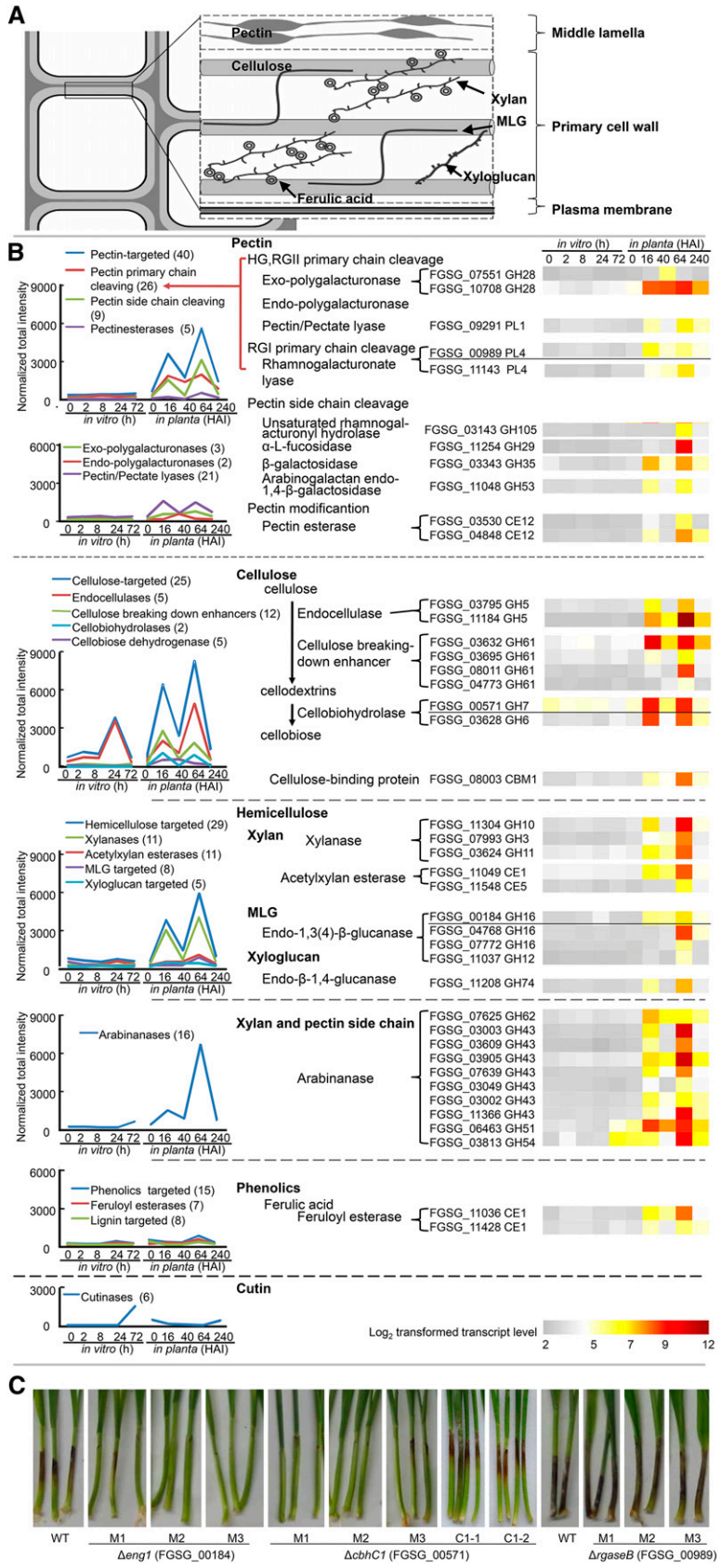

Figure 3. CWDE Gene Expression Increases during Infection, and Two in Planta Preferentially Expressed CWDE Genes Are Required for Virulence in Wheat Coleoptiles.

putative PCWDEs increased almost fivefold at 16 HAI, followed by a nearly twofold reduction at 40 HAI and a subsequent increase of approximately ninefold (Figure 2B; see Supplemental Data Set 4 online). This expression pattern might be related to hyphal growth behaviors (mainly intercellular elongation at 16 HAI, more intracellular growth and branching at 40 HAI, and the complete occupation of the plant cell and the destructive trespassing of plant cell boundaries at 64 HAI), suggesting that there may be a limited digestion of plant cell walls during fungal penetration at 16 HAI and a more extensive digestion of plant cell walls during necrotrophic destruction at 64 HAI.

Considering the context of the host cell wall (i.e., the wheat primary cell wall), we grouped the fungal genes based on the predicted targeted plant cell wall components of the encoded CWDEs (Figure 3A). We first examined CWDEs that target pectin, the major component of intercellular middle lamella. The expression of 26 enzymes that putatively cleave the primary chains of pectin, including endo- and exopolygalacturonases, petin/pectate lyases, and rhamnogalacturonate lyases, was induced at 16 HAI, maintained at a similar level through 40 and 64 HAI and reduced at 240 HAI (Figure 3B). The expression of 25 enzymes that putatively cleave pectin side chains (including 16 arabinanases) only slightly increased at 16 HAI, followed by a more than 10-fold increase at 64 HAI. This expression pattern suggests that at the early stage of infection (16 HAI), *F. graminearum* mainly cleaves the primary chain of pectin, while a more thorough digestion of the pectin side chains and the remaining main chains occurs during later stages (64 HAI).

Next, we examined CWDEs that target cellulose, which functions as a cable-like structural element in the primary cell wall. The expression of 25 cellulose-targeting enzyme genes displayed a similar increase at both 16 and 64 HAI. Interestingly, a group of GH61-type proteins (12), reported to be enhancers of cellulose breakdown (Harris et al., 2010; Quinlan et al., 2011), showed the highest expression levels at 16 HAI (Figure 3B), which is consistent with the idea that this group of enzymes is useful in the initial stage of digesting cellulose surrounded by a hemicellulose sheath.

Among the 32 enzymes putatively targeting hemicellulose, aggregate expression of 11 xylanases showed the most significant increase at both 16 and 64 HAI. Putative feruloyl esterases, which can release cell wall–bound ferulic acids, also displayed increased expression during infection (Figure 3B). Interestingly, the expression of six putative cutinases did not increase during infection, which is consistent with the fact that the epidermal cutin layer was breached by wounding in our experiment.

We individually knocked out three in planta preferentially expressed CWDE genes: FGSG_00989, which encodes a probable rhamnogalacturonase B (RGaseB); FGSG_00571, which encodes a probable cellulose 1,4-β-cellobiosidase (CbhC1) (which was induced 10-fold at 16 and 64 HAI); and FGSG_00184, which encodes a putative endo-1,3(4)-β-glucanase of the GH16 family (Eng1) (see Supplemental Figure 5 online). Mutants lacking *RGaseB*, which encodes a CWDE targeted against pectin, showed virulence similar to the wild type on coleoptiles. This might be because the percentage of pectin in the wheat primary cell wall is low (5%), and there are more than 40 *F. graminearum* genes encoding pectin-targeted enzymes. Knockout mutants for *CbhC1* or *Eng1* showed reduced virulence on coleoptiles (Figure 3C; 40 and 70% reduction in lesion size, respectively). Moreover, two complemented strains of Δ*FgcbhC1* showed similar virulence level to the wild type on coleoptiles.

The frontier of mutant hyphae lacking *CbhC1* or *Eng1* moved inwards more slowly than the wild-type (see Supplemental Figure 5F online). Mutant hyphae at 40 HAI were retained in plant cells close to the cutting edge, usually with one hypha per invaded plant cell, which was similar to the wild type at 16 HAI. At 64 HAI, multiple hyphae were visible in one invaded plant cell, as was the wild type at 40 HAI. It is possible that the plant cell wall network restricted mutant hyphal penetration and extension beginning at 16 HAI when *CbhC1* and *Eng1*were upregulated in wild-type infection.

Fungal Surface Protein Genes Were Induced Both in Vitro and in Planta

Certain cell wall–anchored proteins play a role in sensing environmental signals, and *F. graminearum* may deploy such sensors to respond to host signals (De Groot et al., 2005). *F. graminearum* encodes 46 CPGRP-anchored proteins, a family of putative cell wall–anchored proteins containing the conserved sequence signature [Gly/Ser][Pro/Ala/Val/Asn/Lys/Arg]Cys[Arg/Lys/His/Asn]Pro, as annotated by Ma et al. (2010). Aggregate expression analysis of the CPGRP-anchored gene family revealed transient induction at 16 HAI during coleoptile infection and at 2 to 8 h during in vitro germination (Figure 2B; see Supplemental Data Set 5 online). Moreover, four CPGRP-anchored proteins that also contain an apple (*Malus domestica*) domain (IPR003609) exhibited increased expression at both 16 HAI and 8 h in vitro. An apple domain protein of Apicomplexan parasites is essential for attachment to host cells (Brecht et al., 2001).

Figure 3. (continued).

(A) Schematic diagram (adapted from Vogel [2008]) of the coleoptile cell wall. MLG, mixed linkage glucans.

(B) Expression patterns of cell wall–related genes grouped based on putative targeted substrates. Left panel shows total signal intensities for all genes in the denoted group. The number of genes included in each category is indicated in parentheses. Right panel lists the in planta preferentially expressed gene members in the group and their expression patterns. The genes that were further studied by knockout functional analysis are underlined. HAI, hours after inoculation.

(C) Wheat coleoptile infection assay. M1, M2, and M3 represent independent transgenic lines. C1-1 and C1-2 represent independent complemented strains of M1.

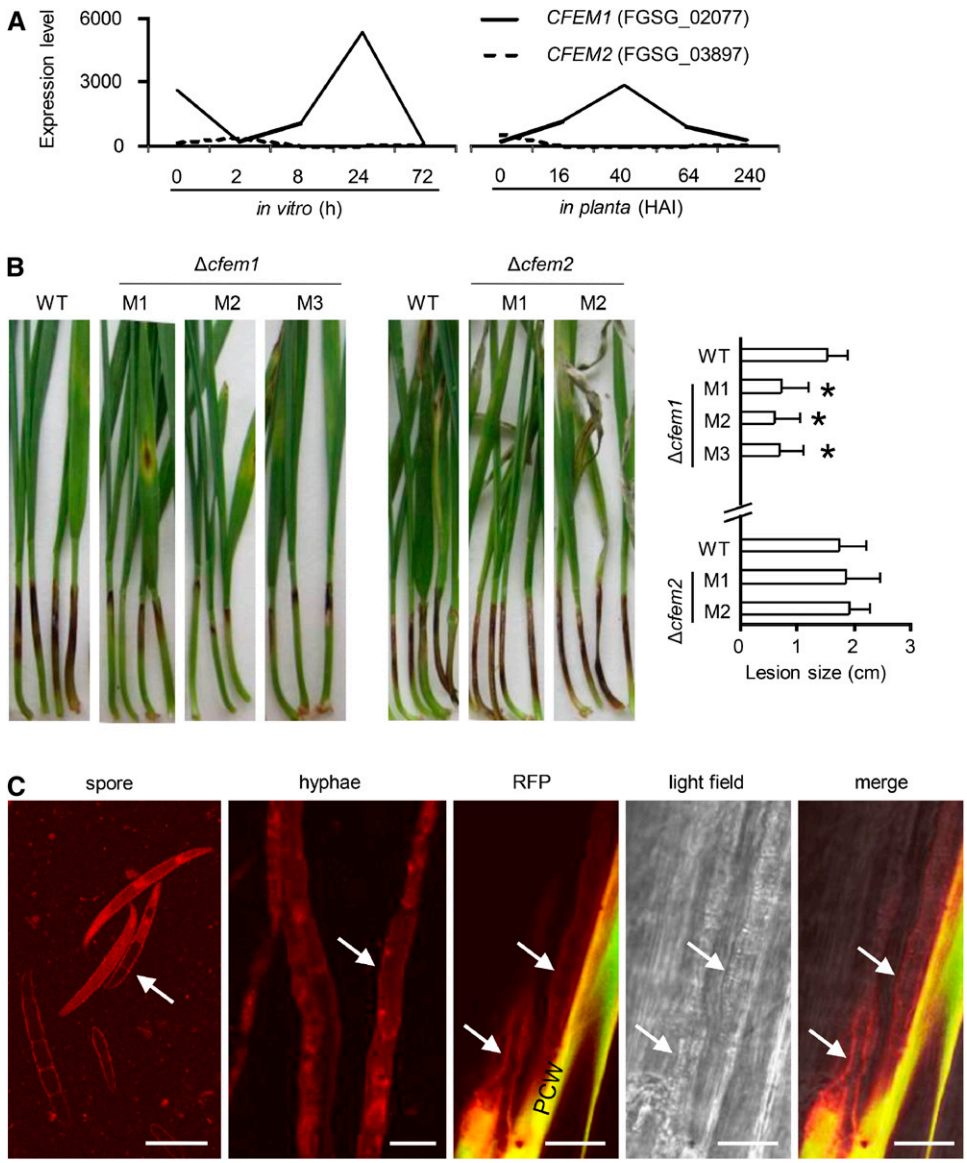

Figure 4. CFEM1 Protein Is Localized on the Fungal Surface, and *CFEM1* Was Required for Full Virulence in a Wheat Coleoptile Infection Assay.

(A) Expression of *CFEM1* and *CFEM2*. HAI, hours after inoculation.

(B) Wheat coleoptile infection assay with the wild type (WT), *CFEM1* deletion mutants (M1, M2, and M3 on left), and *CFEM2* deletion mutants (M1 and M2 on right). Measurements of one representative experiment are shown. Error bars indicate SD (sample size $n = 12$). *Student's t test $P < 0.05$.

(C) Spores of in vitro–grown hyphae and in planta–grown hyphae of *F. graminearum* that express CFEM1-RFP protein. White arrows point to the fungal cell wall. PCW, plant cell wall. Bar = 20 μm.

G protein–coupled receptors (GPCRs) are candidates for recognition of extracellular signals, and of the 116 annotated GPCRs in *F. graminearum* (Ma et al., 2010), 70% (81) were present on the array. The number of GPCR genes expressed at various in planta stages (29, 17, and 22 at 16, 40, and 64 HAI, respectively) was similar to the number of genes expressed at various in vitro stages (ranging from 20 to 38 at 0, 2, 8, 24, and 72 h; see Supplemental Data Set 2 online). Eight GPCR genes exhibited increased expression at 16, 40, or 64 HAI (see Supplemental Data Set 6 online), including two genes encoding putative microbial opsins and six genes similar to *PTH11*, which is a pathogenicity factor in *Magnaporthe oryzae* (DeZwaan et al., 1999).

PTH11-like GPCRs contain an additional N-terminal extracellular membrane-spanning domain (CFEM) that is unique to filamentous ascomycetes (Xu et al., 2006). Besides the six GPCRs, *F. graminearum* encodes 15 additional CFEM proteins. None of the PTH11-type CFEM domain genes showed increased expression during infection. Interestingly, three CFEM proteins belonging to a non-PTH11 subclade were upregulated

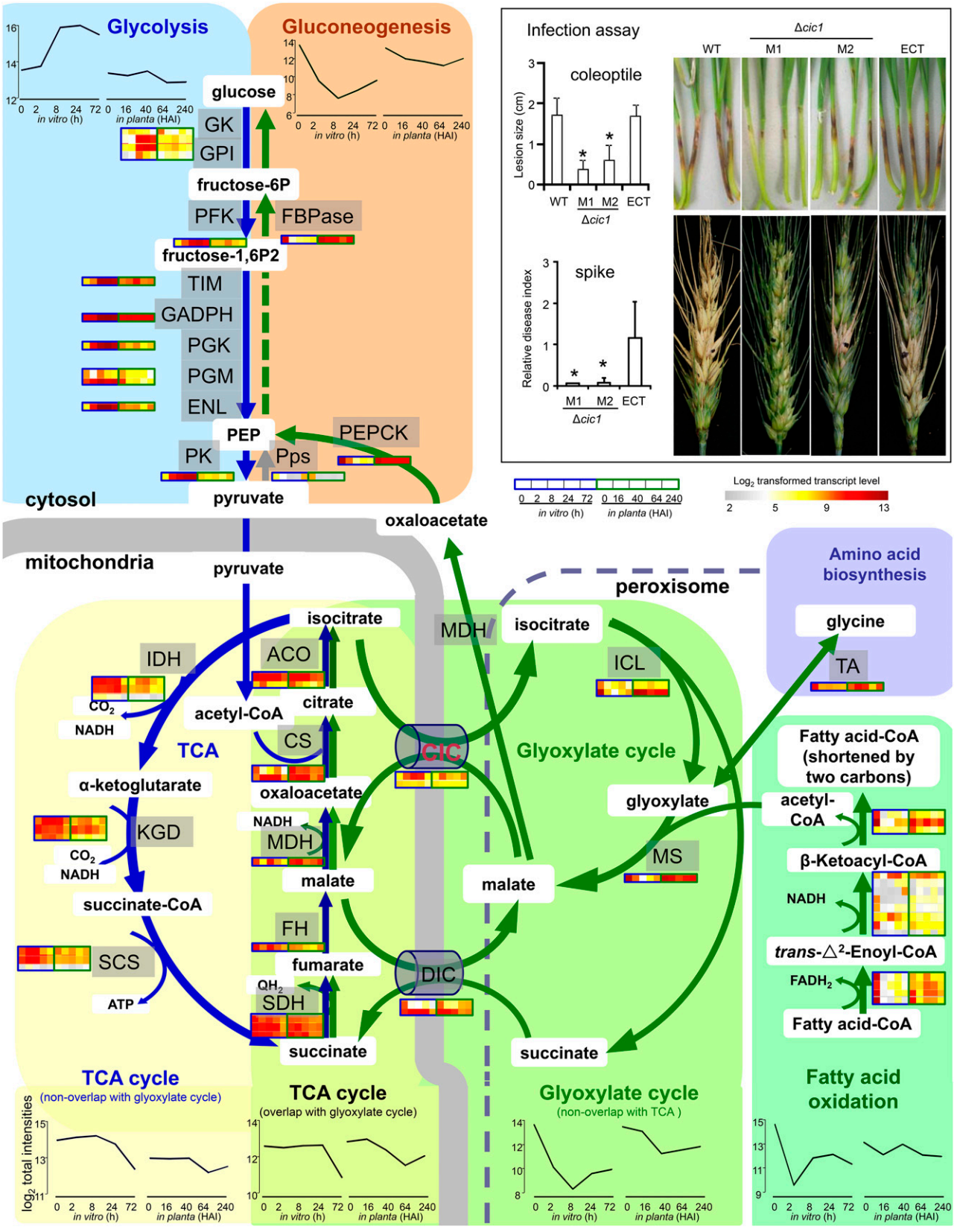

Figure 5. Analysis of Central Metabolic Pathway Gene Expression with Compartmentalization Information.

during infection (Figure 2B; see Supplemental Data Set 7 online). One of these, FGSG_02077 (*CFEM1*), showed increased expression at the early infection stage, and the expression pattern was significantly altered during in vitro growth (Figure 4A). Mutants lacking *CFEM1* showed reduced virulence on coleoptiles (Figure 4B) and reduced hyphal growth in vitro (see Supplemental Figure 5C online). At 16 HAI, mutant hyphae entered into plant cells at the cutting edge, which was similar to the wild-type strain. The difference between the mutant and wild-type strains was evident at 40 HAI. Although the mutant hyphal morphology and growth route preference were similar to those of the wild-type strain, the frontier of mutant hyphae were more restricted to the area near the cutting edge, and fewer hyphae were visible inside the host tissue. At 64 HAI, most hyphae were contained inside the invaded plant cell. Mutant hyphae delayed breaking through the plant cell and grew from one cell to the next (see Supplemental Figure 5F online). We also obtained a knockout strain lacking FGSG_03897 (*CFEM2*), which showed only low expression levels during infection and in vitro growth and had no effect on virulence (Figure 4).

CFEM1 is predicted to be a glycosyl-phosphatidylinositol–anchored protein. Constitutive expression of a CFEM1-RFP (for red fluorescent protein) fusion protein in *F. graminearum* showed that some CFEM1-RFP was localized to the fungal cell surface both in vitro and in planta (Figure 4C), and the CFEM1-RFP signal disappeared from the fungal surface when the cell wall was depleted after protoplastation (see Supplemental Figure 6 online), indicating that CFEM1-RFP is localized to the fungal cell wall. This protein localization pattern is consistent with a possible surveillance role during growth both in planta and in vitro.

Extracellular ROS Scavenging Precedes Production

ROSs are known to be important in pathogen–plant interactions. It is known that ROS can trigger the plant defense response, but the specific role of ROS in fungal pathogenesis is not clear. It is speculated that secreted ROS at toxic levels could act as weapons when necrotrophic pathogens attack the host plant, while at lower levels they might serve as signals to induce the plant defense response (Lamb and Dixon, 1997; Laluk and Mengiste, 2010). A diamino benzaldehyde staining assay (see Supplemental Figure 7A online) showed that at 16 HAI, the infected sites of coleoptiles accumulated more ROS than mock-inoculated coleoptiles at both wounded and nonwounded sites, though wounding per se also induced ROS production in plants. This supports the notion that ROS are involved in the *F. graminearum*–coleoptile interaction. Therefore, we analyzed ROS-related fungal gene expression to determine whether the fungal pathogen contributes to increased or reduced ROS levels.

We first distinguished genes related to extracellular ROS production and scavenging from those involved in intracellular ROS production and scavenging because intracellular ROSs (e.g., in mitochondria and peroxisomes) are more closely associated with cell metabolism and protection against excess self-generated ROS and are not directly relevant to plant–pathogen interactions. *F. graminearum* encodes 28 putative enzymes involved in intracellular ROS production or clearance and 19 putative enzymes involved in extracellular ROS production or clearance (i.e., enzymes that might contribute to changes in in planta ROS levels). Our results (Figure 2C; see Supplemental Figure 7B and Supplemental Data Set 8 online) show that the aggregate transcript levels associated with the expression of extracellular ROS-producing enzymes (including six putative extracellular hydrogen peroxide–producing enzymes and three putative extracellular O_2^--generating NADPH oxidases) did not increase during infection until 64 HAI, and the expression of genes involved in extracellular hydrogen peroxide and O_2^- clearance, including putative catalases and superoxide dismutases, significantly increased at 16 HAI. This expression pattern suggests that *F. graminearum* might keep surrounding ROS levels low to protect itself during the early infection stages (16 and 40 HAI), while producing ROS to compromise surrounding plant cells regardless of the plant defense responses at the late infection stage (64 HAI).

Shift in Primary Metabolism during the Early Stage of Coleoptile Infection

To study the metabolic adjustments that allow fungal growth to occur in planta, we examined the trends in expression levels of genes involved in primary metabolism. We grouped these genes into five categories based on FunCat assignations: oxidative phosphorylation, tricarboxylic acid (TCA) cycle, glycolysis, fatty acid oxidation, and glyoxalate cycle. A comparison of aggregate expression levels over time in vitro versus in planta for these five categories is shown in Figure 2D, and detailed results are shown in Figure 5 and Supplemental Figure 8 online.

For two of the pathways (oxidative phosphorylation and TCA), gene expression trends were similar in vitro and in planta. However, significant differences between in vitro and in planta expression were apparent in three primary metabolic pathways (glycolysis, fatty acid oxidation, and glyoxylate cycle). With in vitro culture, the fatty acid oxidation pathway genes were immediately and sharply reduced in expression (30-fold reduction) at 2 h, and the expression was maintained at a level 10-fold lower than that of the spore stage from 8 to 72 h, while during coleoptile infection, the expression of fatty acid oxidation pathway genes was reduced less sharply (twofold at 16 HAI) and remained at a similar level from 40 to 64 HAI. During in vitro

Figure 5. (continued).

Heat maps in boxes indicate the expression of individual genes, and the chart plots indicate the aggregate expression levels of the pathway genes. The right top inset shows the wheat infection assays of coleoptiles and florets with a deletion of *CIC1*. Measurements of one representative experiment are shown. Error bars indicate SD (sample size $n = 12$). *Student's t test $P < 0.05$. Arrows indicate flux trends inferred from expression patterns. Green arrows, in planta preferred; blue arrows, in vitro preferred. HAI, hours after inoculation.

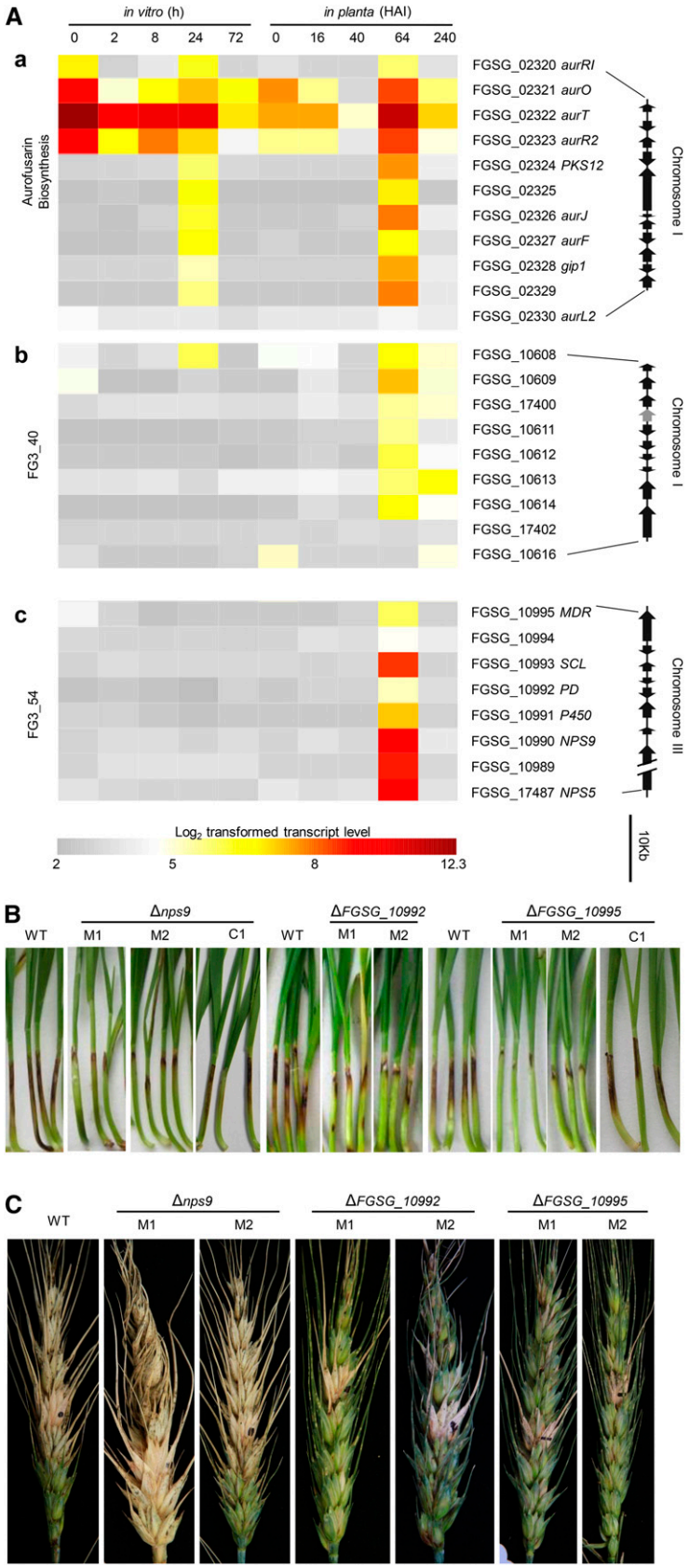

Figure 6. Several SMB Cluster Genes Were Induced during Infection, and the FG3_54 Cluster Is Required for Virulence.

culture, the expression of the glycolysis pathway genes increased significantly (fivefold) after 8 h, and this increased level was maintained at 24 and 72 h; during infection, the expression of glycolysis pathway genes decreased at 16 and 64 HAI. During in vitro culture, glyoxylate-cycle gene expression was reduced twofold after 2 h and remained low at later stages, while during infection, glyoxylate-cycle gene expression was not significantly reduced at 16 HAI and was only slightly reduced at 40 and 64 HAI. The reduction of glyoxylate-cycle gene expression was delayed during infection in comparison with the in vitro situation.

These expression trends suggest that in vitro, *F. graminearum* tends to shut down the fatty acid oxidation pathway, which was active prior to spore germination, relying on glycolysis and the TCA cycle for energy production. By contrast, during the early stages of coleoptile infection (16 HAI), the pathogen tends not to induce glycolysis, but instead it relies on the mobilization of stored lipids through the fatty acid oxidation cycles to form acetyl-CoA, which is further assimilated into the TCA cycle via the glyoxylate cycle. This strategy is consistent with the abundant nutrition sources in the culture medium versus the presumably limited nutrition sources available during early plant infection.

Two key enzymes in the glyoxylate cycle (i.e., isocitrate lyase and malate synthase) are peroxisome localized (Kunze et al., 2006). The branching of the mitochondrial matrix-based citric acid cycle to peroxisome-based glyoxylate bypass should require mitochondrial inner membrane–localized tricarboxylate carriers (such as citrate/malate antiporter) to transport isocitrate from the inner mitochondrial matrix to the cytosol. Our data indicate that *CIC1* (FGSG_01421), one out of the three tricarboxylate transporter genes, increased expression significantly at 16 HAI compared with expression levels found in spores (see Supplemental Data Set 9 and Supplemental Figure 8 online). Knocking out *CIC1* reduced the spore size, but didn't affect in vitro hyphal growth significantly (see Supplemental Figure 9B online). The mutant also reduced lesion size in infected coleoptiles to approximately one-third (Figure 5), and the lesion sizes of complemented strains were similar to that produced by wild-type strains (see Supplemental Figure 5E online). Δ*Fgcic1* hyphae could undergo the same three distinct infection stages as the wild type, but the fungal invaded areas were restricted to neighbor cells at the cutting edge (see Supplemental Figure 5F online).

Specific Secondary Metabolite Clusters Were Induced at 64 HAI

In addition to proteins, small molecules, such as secondary metabolites, may function as effectors of pathogenicity (Wolpert et al., 2002). We examined the pathway genes of well-characterized mycotoxins, including trichothecene (Alexander et al., 2009), zearalenone (Kim et al., 2005; Gaffoor and Trail, 2006), and aurofusarin (Malz et al., 2005). Our expression data show that almost no DON biosynthesis genes were induced during the infection of coleoptiles (Figure 2E; see Supplemental Figure 10 online), suggesting that *F. graminearum* might not employ DON releasing as a coleoptile infection strategy. Similarly, the five genes involved in synthesizing the polyketide mycotoxin zearalenone were not induced during coleoptile infection either (see Supplemental Data Set 10 online).

The expression of genes involved in the biosynthesis of the polyketide pigment aurofusarin was increased significantly at 64 HAI (Figure 2E; see Supplemental Figure 11 online). Knocking out the main regulator of the aurofusarin cluster, *aurRI*, abolished pigmentation during in vitro culture, but it didn't reduce virulence (see Supplemental Figure 11 online). This is not surprising given that aurofusarin biosynthesis gene expression levels also increased during in vitro culture (Figure 6A, panel a).

Fungal secondary metabolite biosynthetic (SMB) pathway genes often occur in contiguous gene clusters, which often include genes encoding nonribosomal peptide synthetase (NPS) or polyketide synthase. Based on gene composition and coexpression patterns, 15 SMB gene clusters have been annotated even in the absence of information about the products (Ma et al., 2010). Among these, only the FG3_40 cluster genes showed significant upregulated coexpression of the entire gene cluster during coleoptile infection (Figure 6A, panel b; see Supplemental Data Set 10 online).

We screened all of the predicted NPS and polyketide synthase genes that had more than two flanking genes showing a similar expression pattern under 15 diverse conditions and located four additional coexpressed gene clusters that are hypothetically involved in secondary metabolite biosynthesis. One of these, FG3_54, comprises eight genes, all of which were specifically induced at 64 HAI (Figure 6A, panel c; see Supplemental Data Set 10 online). This gene cluster locus includes two putative NPS genes. NPS5 (encoding 11,198 amino acids), composed of five full adenylation (A)–pantothenylation (P) –condensation (C) modules. NPS9 contains only A and P domains. Also in this cluster, FGSG_10993 encodes a putative selenocysteine lyase, while the FGSG_10992 protein is similar to a peptidoglycan deacetylase. FGSG_10991 encodes a putative benzoate 4-monooxygenase cytochrome P450, and FGSG_10995 encodes a putative multidrug resistance protein that might function as an efflux transporter. Mutants with NPS9, FGSG_10992, or FGSG_10995 deleted individually all showed reduced virulence during coleoptile infection, among which the FGSG_10995

Figure 6. (continued).

(A) Heat maps showing the expression of genes in three SMB gene clusters. The corresponding chromosome localization is shown on the far right. The gray arrow indicates that the gene was not included in the GeneChip. MDR, multidrug resistance protein; P450, benzoate 4-monooxygenase cytochrome P450; PD, polysaccharide deacetylase; SCL, selenocysteine lyase. hpi, hours post inoculation.

(B) Coleoptile infection assay. M1 and M2 represent independent transgenic lines. C1, complemented line.

(C) Wheat floret infection assay.

mutants produced the least lesion development (Figure 6B). When the wild-type *NPS9* and FGSG_10995 alleles were transformed into the Δ*nps9* mutant and the Δ*FGSG_10995* mutant, respectively, defects in coleoptile infection were rescued (Figure 6B), indicating that the deletion of *NPS9* and FGSG_10995 was responsible for virulence reduction. Hyphae of the three mutants showed a similar infection process from 16 to 64 HAI to PH-1 and invaded aggressively. After 64 HAI, the hyphae of Δ*Fgnps9* and Δ*FGSG_10995* were still restricted to the cell wall–thickened plant cells and didn't break out, while some Δ*FGSG_10992* hyphae could break out and penetrate the next plant cell (see Supplemental Figure 5F online). However, the frequency of breaking out was lower in Δ*FGSG_10992* hyphae than in wild-type hyphae. Our results further suggest that the unknown product of the FG3_54 cluster that specifically accumulated after 64 HAI contributes to infection. Based on the composition of the cluster gene, we speculate that the unknown product could be a nonribosomal peptide, possibly toxic, that was exported out of the fungus during the late stage of infection.

DISCUSSION

Among the stages of fungal infection (germination/penetration, proliferation, and sporulation), the proliferation stage is arguably the least well understood, as it is the least accessible to direct study. Using laser capture microdissection and a cut coleoptile as the infection site, we obtained high-resolution gene expression profiles that delineate at least three discrete stages during *F. graminearum* proliferation inside the host plant tissue. The three stages of infection are represented by three time points, based on our sampling scheme: 16, 40, and 64 HAI. The infection strategies inferred from our observations, and elaborated in the discussion below, are listed in Supplemental Figure 12 online. While much evidence already points to the use of CWDEs and toxins during pathogenesis (Walter et al., 2010; Kazan et al., 2012), our study delineates a time frame for these events. We propose two phases of CWDE accumulation: (1) targeting preferentially the main chains of cell wall components and (2) a more extensive round encompassing the digestion of side chains. Secondary metabolites, such as aurofusarin and the product of FG3_54 cluster enzymes, are primarily produced at the late stage of infection (64 HAI). Producing ROS in the surrounding plant tissue occurs later than ROS clearing. In line with Laluk and Mengiste (2010), who characterized necrotrophic attacks on plants as either "wanton destruction" or "covert extortion," we propose to call the first (16 HAI) and third (64 HAI) stages of infection "covert penetration" and "overt destruction", respectively (Figure 1C).

Concerning the relationship between host cell death and hyphal growth, besides expression analysis, a plasmolysis assay (see Supplemental Figure 13 online) indicates that at 16 HAI, host cells in the wake of fungal advance may have already been dying, although the cells adjacent to the hyphal tips appeared normal. Also, on close observation, cell wall deposition appeared to occur from the neighbor cell side but not the invaded-cell side (Figure 1B; see Supplemental Figure 2 online). In conclusion, *F. graminearum* begin to cause death in the invaded host cell as early as 16 HAI, possibly by penetrating the host's cell wall and physically occupying the cell; the pathogen starts to kill surrounding plant cells that it has not yet invaded at 64 HAI by secreting toxic chemicals and extensively digesting the plant cell walls. Therefore, our work provides additional insight into the onset of host cell destruction by *F. graminearum*.

At 40 HAI, *F. graminearum* hyphae continued to grow within the host cell (Figure 1), which is consistent with the reduction of PCWDE expression (Figure 2B). A putative cell wall–bound invertase (FGSG_02339) and five putative plasma membrane Glc transporters, increased in expression significantly at 40 HAI over levels observed at 16 HAI. Suc is the major transport carbon form in plants. By secreting Suc-cleaving invertases to the apoplast and increasing glucose transporters at the local cell membrane, plants can define an organ (such as a developing seed) as a carbohydrate "sink" (Sturm and Tang, 1999). *F. graminearum* might use this strategy to obtain carbon from other parts of the host. The hyphae at this stage had more branches at the tip, which is expected to increase surface area and might be related to improving the importing of nutrients. At 40 HAI, the expression of two key enzymes involved in gluconeogenesis (FBPase and PEPCK) was significantly higher (fivefold) than in vitro levels, and glycogen synthase expression was similar to that observed during in vitro growth, which occurs among an abundant supply of nutrients (see Supplemental Figure 8 online). These expression trends of actively producing Glc and glycogen suggest fairly aggressive fungal growth at 40 HAI. Therefore, we propose to call the 40 HAI the stage of pathogen infection "rapid proliferation."

Analyzing primary metabolic pathway gene expression has enabled us to suggest that *F. graminearum* delays the switching off of fatty acid oxidation and enhances the glyoxylate cycle to survive Glc starvation during early infection. A similar glyoxylate cycle-enhancing strategy has been reported for *Candida albicans* infection (Lorenz and Fink, 2001) and *M. oryzae* infection (Wang et al., 2003). In the pathogen *Fusarium oxysporum*, FOW1, which shares 98% identity with CIC1, was shown to be important for virulence (Inoue et al., 2002). However, it was unclear how a mitochondrial protein that is not required for saprophytic growth could specifically function in pathogenesis. Our investigation suggests that the transport of isocitrate out of the mitochondria by CIC1 is a step in the glyoxylate cycle that should be enhanced during early infection.

Our microarray data were validated in a number of ways. First, we chose 28 genes for real-time PCR verification. At each of the six time points examined by microarray analysis, the 28 chosen genes were examined by real-time PCR. We found that the real-time PCR results, in which 80% (16 out of 20) of the genes were moderately to highly expressed, were consistent with the microarray data. In addition, the real-time PCR results showing that 50% (four out of eight) of the genes had low expression levels were consistent with the microarray data (see Supplemental Figure 14 online). Second, we detected aurofusarin in 64-HAI infected coleoptiles, as predicted by pathway gene expression analysis (see Supplemental Figure 11 online). Third, among the 22 genes selected for genetic deletion based on in planta expression patterns, eight (36%) caused

a significant reduction of virulence in coleoptiles (see Supplemental Figure 5 online).

F. graminearum typically causes head blight due to floret infection (see Supplemental Figure 15 online). To obtain synchronized samples, we studied coleoptile infection. Whether strategies for coleoptile infection are similar to those for floret infection is of interest. The expression of trichothecene biosynthesis genes did not increase during coleoptile infection (see Supplemental Figure 10 online), while the increasing expression of these genes is important for floret infection. On the other hand, the expression of aurofusarin synthesis genes increased during both coleoptile infection and in vitro culture, while the expression of these genes has not been reported to be increased on florets. FG3_54 SMB cluster genes all exhibited increased expression at 64 HAI on coleoptiles, while a member of this cluster, *NPS9*, also increased expression at 96 HAI during floret infection (Lysøe et al., 2011). Among the 133 *F. graminearum* genes known to be required for wheat floret infection, 17 genes increased expression on coleoptiles, while the expression of 11 genes was not detected in any of our microarray hybridization (see Supplemental Figure 16 online). Among the seven genes required for full virulence on coleoptiles, the CFEM protein FGSG_02077 is required for floret infection (Dufresne et al., 2008). The mutant strains lacking the mitochondrial carrier CIC1 or one of two gene members of the FG3_54 cluster (FGSG_10992 or FGSG_10995) also displayed reduced virulence on florets (Figure 6; see Supplemental Figure 17 online), while the mutant strains lacking the CWDEs (*CbhC1* and *Eng1*) or another member of the FG3_54 SMB cluster *NPS9* didn't reduce virulence on florets significantly. In line with organ specificity of virulence genes demonstrated in the *Ustilago maydis*–maize system (Skibbe et al., 2010), the three genes required for coleoptile infection but not for floret infection might represent virulence genes specific to coleoptile infection.

METHODS

Wheat Infection and Microscopy Observation

Transgenic *Fusarium graminearum* strain PH-1 (NRRL 31084) expressing the AmCyan protein driven by the strong constitutive vma3 promoter was previously obtained (Yuan et al., 2008). This strain, AmCyanPH-1, has similar growth characteristics to wild-type PH-1 during both in vitro culture and plant infection (see Supplemental Figure 18 online).

To prepare conidial suspensions for inoculation, AmCyanPH-1 conidia, maintained as glycerol stocks at −80°C, were placed into V8 juice agar and grown for 1 to 2 weeks at room temperature. Falcate conidia collected from V8 agar plates were then transferred into liquid mung bean medium and cultivated at 25°C for 3 d with shaking at 150 rpm. The conidial suspension was filtered through Miracloth and centrifuged at 8000 rpm for 10 min. The harvested conidia were resuspended in sterile water and adjusted to 10^7/mL. The suspension was used for inoculation within 2 h. Sterile cotton strips (4 mm × 1 cm) were soaked in the conidial suspension.

Three-day-old seedlings of wheat (*Triticum aestivum*) cultivar Zhongyuan 98-68 (susceptible to *F. graminearum* and widely cultured in Henan, China) were used for the coleoptile infection assay according to Wu et al. (2005) with modifications. Three days after seed sowing, the top 2 to 3 mm of the coleoptiles were removed, and the seedlings were wrapped in 4 mm × 1-cm cotton strips and incubated for 3 d (see Supplemental Figure 2A online). Mock-inoculated coleoptiles (with water) served as controls. After inoculation, the seedlings were grown in a growth chamber at 25°C and 95% humidity.

At time points spanning 0 to 10 DAI, inoculated seedlings were examined using an Olympus BX51 microscope equipped with a green fluorescent protein filter set (450- to 480-nm excitation; 515-nm emission). Confocal images were acquired on an Olympus Fv10i or Fluoview FV1000 microscope with two emission-collecting windows operating simultaneously. Excitation/emission wavelengths were 405 nm/460 to 500 nm for AmCyan and 405 nm/570 to 670 nm for plant cell wall autofluorescence. The images were merged using Image-Pro software (Media Cybernetics). All fluorescence microscopic pictures presented in this study are confocal images except for those labeled with "e" (epifluorescence images).

Tissue Preparation and Laser Capture Microdissection

F. graminearum–inoculated and mock-inoculated coleoptiles at 16, 40, 64, and 240 HAI were fixed and paraffin embedded as previously described by Tang et al. (2006), except that xylene was used in place of histoclear II. After vacuum infiltration, the fixative was replaced with fresh ice-cold acetone before microwaving. Ten-micrometer-thick sections were obtained using a rotary microtome (Leica RM2235; Leica Biosystems Nussloch). To enhance RNA preservation, a paraffin tape transfer system (Instrumedics) was employed (Cai and Lashbrook, 2006).

Prior to laser capture microdissection, the slides were illuminated for 1 min under the ultraviolent lamp (366 nm) of the paraffin tape transfer system and deparafinized twice in xylene, 5 min each time, and air dried for 2 to 3 h. The slides were then loaded into a Veritas Microdissection Instrument (Acturus Bioscience). The AmCyan-tagged fungal hyphae inside wheat tissues on the slides were captured using the following settings: spot size, 10 to 20 μm; power, 100 mW; and pulse duration, 2.5 to 4 ms. The hyphae of interest (at least 1 mm away from the wounded sites) were isolated. Approximately 100,000 μm^2 of tissue was obtained for each sample. The sample at 240 HAI was scraped directly from the slides.

RNA Extraction, Amplification, and Microarray Hybridization

For the 16, 40, 64, and 240 HAI samples, total RNA was extracted using a PicoPure RNA isolation kit (Acturus) and subjected to DNase (RNase-free DNA set; Qiagen) treatment according to the manufacturer's protocol. Next, 10 μg of biotinylated complementary RNA (cRNA) was generated using an Affymetrix Two-Cycle Target Labeling Assay Kit (Affymetrix) combined with a MEGAscript High Yield Transcription Kit (Ambion AM1333), according to the protocol described in the GeneChip Expression Analysis Technical Manual.

The conidial suspensions for wheat inoculation were centrifuged to obtain pellets, which were used as the 0 HAI conidia samples. To prepare samples of hyphae grown in vitro for 72 h, the falcate conidia collected from the V8 agar plates were transferred to a yeast extract peptone dextrose liquid medium and cultivated at 25°C for 3 d with shaking at 150 rpm. For in vitro–cultured conidia and hyphae, total RNA was extracted using Trizol (Invitrogen), diluted to 1 ng/μL, and amplified as above.

The quality of RNA samples was assessed using an RNA 6000 Pico Assay Kit with an Agilent 2100 Bioanalyzer (Agilent Technologies). The quantity of laser capture microdissection–derived RNA was estimated with an Agilent 2100 Bioanalyzer by employing standard RNA samples of 1 ng. The quantities of Trizol-isolated or amplified RNA were estimated using a Biophotometer (Eppendorf North America).

Chip hybridization, washes, and chip reading were performed at ShanghaiBio with cRNA using an *F. graminearum* Affymetrix GeneChip (Güldener et al., 2006) according to the manufacturer's protocol. Three biological replicates were obtained for each time point, except for 240 HAI, which had two biological replicates.

Microarray Data Processing

Original CEL files were normalized by Robust Multichip Analysis (RMA) with Bioconductor R software using the "rma" function of the affy package. Correlation coefficients between biological replicates (see Supplemental Figure 4A online) were ~0.96, and the average correlation coefficient for LM-derived samples was 0.94 (ranging from 0.90 to 0.99, SD 0.038). A presence/absence test was conducted with the detection quality P value < 0.004. A gene was called present (P) if P value < 0.004 in at least two biological replicates. A gene was considered absent (A) if P value > 0.065 in at least two biological replicates. The detection ratios for each chip were ~49%. Microarray data were deposited in the Plexdb database (http://www.plexdb.org/; Dash et al., 2012) under accession number FG19: stage-specific expression patterns of *F. graminearum* growing inside wheat coleoptiles with LM.

Because two-round T7-based RNA amplification was performed to obtain RNA samples for chip hybridization, the derived cRNAs were limited to ~500 nucleotides from the 3′ terminus (Tang et al., 2012). Probe sets for the *F. graminearum* GeneChip were designed using the first genome assembly version. All probe-covering sequences were used to BLAST against the current version FG3 gene sequence (Wong et al., 2011), and the probe sets with complementary sequences not within 500 nucleotides of the 3′ terminus of the corresponding genes were omitted. Also, for each gene, only one representative probe set was chosen as a uniprobe set to avoid redundancy in follow-up enrichment analysis. In total, of the 18,069 probe sets in the chip, 13,429 probe sets, representing 13,429 *F. graminearum* unigenes, were chosen for further analysis.

Probe sequence similarity with host plants, including wheat, was taken into consideration in the original *F. graminearum* GeneChip design (Güldener et al., 2006); however, the complete genome sequence of wheat is still lacking. To ensure the probe specificity in detecting fungal RNA in wheat, plant cells from mock-inoculated wheat coleoptiles were laser captured to hybridize to the *F. graminearum* GeneChip with three biological replicates. Among 13,429 uniprobe sets, only two probe sets, FGSG_06541 (fgd259-1440_at) and FGSG_17540 (fgd468-150_at), were called as present in two biological replicates at a detection P value < 0.004 level and were therefore excluded from later analysis to avoid cross-hybridization from the wheat coleoptile in the laser-captured samples.

To compare in vitro data with in planta expression data, CEL files of *F. graminearum* gene expression profiles during the conidia germination stages (Seong et al., 2008) were downloaded from Plexdb, and Robust Multichip Analysis normalization was performed on 29 combined microarray data sets at 10 time points (in vitro: 0, 2, 8, 24, and 72 h; in planta: 0, 16, 40, 64, and 240 HAI). A total of 344 in planta preferentially expressed probe sets with false discovery rates < 0.05 were defined as follows: first, a fold change cutoff of 1.5-fold was applied to the 13,427 uniprobe sets, resulting in 569 probe sets with expression levels in at least one of the three in planta time points (i.e., 16, 40, or 64 HAI) that were higher than those obtained in any of the non–in planta conditions, including the spore (0 HAI) and hyphae (72 h) and previously published in vitro results at 0, 2, 8, and 24 h (Seong et al., 2008); next, a P value cutoff of 0.004 was combined with the above fold change cutoff to calculate the expected number of significant probes = 569 * 0.004 * 6 = 13.7, with Bonferroni correction used to correct for the multiple comparison; third, the number of probes that met the combined thresholds is 344, corresponding to an apparent false discovery rate = 13.7/344 = 0.04.

Expression Data Analysis

FunCat (Ruepp et al., 2004) annotations for *F. graminearum* genes were downloaded from FGDB (ftp://ftpmips.gsf.de/FGDB/). FunCat family enrichment assays for each time point for expressed genes and differentially expressed genes (separated for increase and reduction in expression) were performed using the χ^2 test. For KEGG pathway enrichment analysis, KegArray software was employed (http://www.genome.jp/kegg/download/kegtools.html). The aggregate intensity of all the members in the family or pathway was examined (by adding the average normalized PM value of the probe set representing each member gene) to uncover common expression patterns for the entire family or pathway, followed by checking the expression levels of individual genes in the family or group. Expression heat maps were generated in Bioconductor R using the "heatmap" function of the amap package. Hierarchical cluster analysis and principal component analysis were performed using GeneSpring GX 7.3 (Silicon Genetics, Agilent Technologies) with imported CEL files.

The lists of putative secreted proteins, CPGRP-anchored proteins (see Supplemental Data Set 5 online), and GPCR (see Supplemental Data Set 6 online) use the annotation of Ma et al. (2010). CFEM domain–containing proteins (see Supplemental Data Set 7 online) were obtained from FGDB. Genes related to ROS production and scavenging (see Supplemental Data Set 8 online) were annotated based on the enzyme commission number annotated on KEGG (http://www.genome.jp/kegg/) and FGDB.

Genes involved in cell wall degradation (see Supplemental Data Set 4 online) were manually annotated with reference to the Carbohydrate-Active Enzymes (CAZy; www.cazy.org) annotation for *F. graminearum* genes by Ma et al. (2010). These proteins were further categorized according to the predicted substrates and category of carbohydrate-cleaving family (Duplessis et al., 2011).

Information concerning 18 SMB gene clusters was obtained from Ma et al. (2010). To identify additional SMB clusters, the coexpression correlation coefficients of all the annotated terpene synthase, polyketide synthase, or nonribosomal peptide synthetase genes were calculated with their flanking genes on the chromosome. Four loci had correlation coefficients among at least three genes that were higher than 0.89. These genes were designated as SMB clusters FG3_51 to FG3_54.

Generation of Fungal Mutants

The split marker recombination procedure (Catlett et al., 2003) was used to generate knockout mutants. Supplemental Data Set 11 online provides the primer sequences. The newly derived PCR products were transformed into protoplasts of wild-type PH-1, and the resulting hygromycin-resistant transformants were screened using genomic DNA PCR and verified by DNA gel blot analysis (see Supplemental Figure 5A online).

For complementation assays, a fragment containing the gene and promoter region was amplified and cloned into pTG19. The fragment was then cloned into a vector with a neomycin resistance cassette. The resulting constructs were transformed into protoplasts of the mutants.

The Fg-*CFEM1* (FGSG_02077) full-length cDNA was cloned into the vma3 promoter-mRFP vector (Yuan et al., 2008) to generate a fungal constitutively expressed FgCFEM1-mRFP construct. The transformants were verified using PCR and fluorescence under a long-pass RFP filter set (510- to 550-nm excitation; 590-nm emission).

Infection Assay for Virulence Assessment

For the coleoptile infection assay, Zhongyuan 98-68 wheat seeds were planted in 24-well plates, one seed per well, with filter paper to retain moisture. Three days after sowing, the top 2 to 3 mm of the coleoptiles were removed, and fresh conidia (10^6/mL) from mung bean (*Vigna radiata*) liquid were pipetted directly onto the wounded seedlings. This resulted in a water drop swinging on top of the coleoptiles. The inoculated wheat coleoptiles were placed in a growth chamber with a 12-h-day/12-h-night light cycle at 25°C. After photography at 10 DAI, the lesion length was measured using ImageJ software and evaluated using Student's *t* test. At least two independent knockout lines were used for each gene, and at least 12 wheat seedlings per mutant were evaluated in at least two independent experiments.

Bobwhite spring wheat was used in the floret infection assay. According to Wang et al. (2011), flowering wheat heads were drop-inoculated with 10 μL fresh conidia (10^6/mL) into the floral cavity between the lemma and palea in the middle floret on the spike. Control plants were mock inoculated with distilled water. After inoculation, the treated wheat heads were sprayed with water and covered with plastic bags to produce high humidity for 48 h. For each fungal strain, two independent experiments were performed. At least six wheat heads were examined in each repeat per strain. Disease was rated by the number of symptomatic spikelets at 14 DAI.

Quantitative RT-PCR

The total RNA samples were amplified to generate antisense RNAs using a TargetAmp two-round aminoallyl-aRNA amplification kit (Epicentre Biotechnologies) and treated with an RNeasy MinElute Cleanup Kit (Qiagen) according to the manufacturer's instructions. The cDNAs were prepared using reverse transcriptase M-MLV (TaKaRa Biotechnology) according to the manufacturer's protocol. Quantitative PCR experiments were performed using a Bio-Rad MyiQ single-color real-time PCR detection system with SYBR Green reaction mix comprising 2 μL of template (~20 ng), 10 μL of 2× SYBR green premix, 0.4 μL of forward primer (10 μM), 0.4 μL of reverse primer (10 μM), and 7.2 μL of nucleotide-free water. The PCR program used was as follows: an initial denaturation step at 95°C for 30 s followed by 40 amplification cycles at 95.0°C for 5 s and 60°C for 30 s. After completion, a melting curve was constructed by increasing the temperature from 72 to 95°C by slowly increasing the temperature by 0.5°C/s and holding 8 s at each temperature. To ensure specificity, only primers that generated a single peak in the melting curve were selected. Primer sequences are listed in Supplemental Data Set 11 online. A serial template dilution for each pair of primers was included to generate standard curves for calculating reaction efficiency. The β-tubulin gene (FGSG_09530) was used as a reference. To monitor contamination, mock (using water as a template) reactions were performed for all genes in each experiment. Each experiment included three biological replicates for each pair of primers and was repeated at least twice.

Autofusarin Extraction and Detection

We collected infected parts of ~200 wheat coleoptiles and similar parts of ~200 mock-inoculated coleoptiles at 64 HAI, as well as 1-week-old hyphae (~200 mg) cultured in V8 solid medium. Samples were ground thoroughly in liquid nitrogen and then extracted with 500 μL methanol-dichloromethane-ethyl acetate solvent mixture (1:2:3, v:v:v) containing 1% (v/v) formic acid. After 20 min of ultrasonication, the upper organic phases were transferred to new vials and evaporated to ~100 μL under a gentle stream of nitrogen.

Aurofusarin was detected by liquid chromatography (LC)–UV–electrospray ionization (ESI)–mass spectrometry (MS). Six-microliter samples were injected into Agilent accurate-mass quantitative time-of-flight (Q-TOF) LC-MS system (model G6520A) equipped with a diode array detector. An Agilent Zorbax XDB-C18 column (4.6 × 50 mm, 1.8 μm) was used for LC separation with binary solvents: 0.1% formic acid in water (v/v) as solvent A and methanol with 0.1% formic acid (v/v) as solvent B. The following gradient program was used: 30% B kept isocratic for the first 2 min and then solvent B was ramped to 100% over 20 min and then down to initial 30% B and kept 3 min to recondition the column. The LC flow rate was set to 0.2 mL/min. Aurofusarin was monitored by the diode array detector at 240 nm and by the Q-TOF operated under negative ESI and full scan mode. The ESI source parameters of Q-TOF are following: nebulizer pressure 276 kPa, drying gas (N_2) temperature 350°C and flow rate 9 L/min, ESI Vcap 3500 V, fragmentor voltage 160 V, skimmer voltage 65 V, and Otc RF Vpp voltage 750V. The mass range was set to 40 to 650 mass-to-charge ratio.

Autofusarin was confirmed by a UV peak at ~18 min and its corresponding peak appeared in the extracted ion chromatograph with 569.079 mass-to-charge ratio, which could correspond to aurofusarin (formula: C30H18O12, calculated accurate mass for M-H-: 569.07255, measured mass: 569.079, error: 11.3 ppm). Aurofusarin was further confirmed by matching measured versus predicted isotopic distribution of 569.08, 570.08, and 571.08 (see Supplemental Figure 11 online).

Accession Numbers

GenBank accession numbers of genes used in this article are as follows: XM_380360 for *Eng1* (FGSG_00184), XM_380747 for *CbhC1* (FGSG_00571), XM_381165 for *RGaseB* (FGSG_00989), XM_382253 for *CFEM1* (FGSG_02077), XM_384073 for *CFEM2* (FGSG_03897), XM_391164 for *NPS5* (FGSG_17487), XM_391165 for FGSG_10989, XM_391166 for *NPS9* (FGSG_10990), XM_391167 for FGSG_10991, XM_391168 for FGSG_10992, XM_391169 for FGSG_10993, XM_391170 for FGSG_10994, XM_391171 for FGSG_10995, and XM_381597 for *CIC1* (FGSG_01421). Microarray data were deposited in the Plexdb database (http://www.plexdb.org/) under accession number FG19.

Supplemental Data

The following materials are available in the online version of this article.

Supplemental Figure 1. Wheat Coleoptile Comprises Similar Cells and Can Be Infected by *F. graminearum* without Wounding.

Supplemental Figure 2. The Progression of AmCyanPH-1 inside Wheat Coleoptile after Inoculation through a Cut Site.

Supplemental Figure 3. The Progression of AmCyanPH-1 That Entered the Host through Stomata.

Supplemental Figure 4. General Information about the Microarray Data.

Supplemental Figure 5. Verification and Phenotypic Characterization of *F. graminearum* Mutants.

Supplemental Figure 6. Protoplastation of *F. graminearum* Expressing CFEM1-RFP.

Supplemental Figure 7. ROSs Are Involved in the *F. graminearum*–Wheat Interaction.

Supplemental Figure 8. Detailed Expression Patterns of Central Metabolic Pathways.

Supplemental Figure 9. Phenotypic Characterization of Δ*Fgcic1* Mutants.

Supplemental Figure 10. Expression of Genes in the Trichothecene Biosynthetic Pathway.

Supplemental Figure 11. Detection of Aurofusarin and Coleoptile Infection Assays of Aurofusarin Biosynthetic Mutants.

Supplemental Figure 12. Features of the Three Stages of *F. graminearum* Proliferation inside Wheat Coleoptiles.

Supplemental Figure 13. Plasmolysis Assay of Infected Coleoptile Cells.

Supplemental Figure 14. Quantitative RT-PCR Analysis of 28 *F. graminearum* Genes.

Supplemental Figure 15. Growth of AmCyanPH-1 in Wheat Spikes at 7 dpi.

Supplemental Figure 16. Coexpression Patterns during Coleoptile Infection of 133 *F. graminearum* Genes Known to Be Required for Pathogenicity on Wheat Florets.

Supplemental Figure 17. Virulence of *F. graminearum* Mutants on Wheat Heads.

Supplemental Figure 18. AmCyanPH-1 Strain Is Similar to PH-1.

Supplemental Data Set 1. Expression Patterns of in Planta Preferentially Expressed Genes.

Supplemental Data Set 2. Summary of Expressed Gene Numbers in Various Categories.

Supplemental Data Set 3. FunCat Enrichment Analysis.

Supplemental Data Set 4. Expression Patterns of Plant Cell Wall Penetration/Digestion-Related Genes.

Supplemental Data Set 5. Expression Patterns of Predicted CPGRP Anchored Protein Genes.

Supplemental Data Set 6. Expression Patterns of G-Protein Coupled Receptor Genes.

Supplemental Data Set 7. Expression Patterns of CFEM Protein Genes.

Supplemental Data Set 8. Expression Patterns of Putative ROS-Producing and Scavenging Enzyme Genes.

Supplemental Data Set 9. Expression of Genes Involved in Central Metabolism Pathways.

Supplemental Data Set 10. Expression Patterns of Secondary Metabolite Biosynthesis Cluster Genes.

Supplemental Data Set 11. Primers Used in This Study.

ACKNOWLEDGMENTS

This work was supported by National Basic Research Program of China (2011CB100702), the Chinese Academy of Sciences Knowledge Innovation Program (KSCX2-EW-N-06), and the Ministry of Agriculture (2011ZX08009-003). W.-H.T. acknowledges support from the SA-SIBS Scholarship Program. We thank Jon Duvick, Sheila McCormick, Jin-Rong Xu, Zhihua Zhou, Laigen Li, Chen Yang, and Chengshu Wang for critical review of the article, Yijing Zhang for advice on statistics, Daolin Fu for help with floret infection, Yining Liu and Shilan Zhao for instruction in LC-MS, Hua-Sheng Xiao for improving RNA labeling for microarray analysis, Zonghua Wang and Youliang Peng for instructions on generating knockouts, and Shu-Jie Wang and Sheng-Hua Yao for assistance in article preparation.

AUTHOR CONTRIBUTIONS

W.-H.T. and D.Z. designed experiments. X.-W.Z, L.-J.J., Y.Z., and D.Z. performed experiments. W.-H.T., X.-W.Z, X.L. and G.J. analyzed data. W.-H.T. and X.-W.Z. wrote the article.

Received October 5, 2012; revised November 24, 2012; accepted December 7, 2012; published December 24, 2012.

REFERENCES

Alexander, N.J., Proctor, R.H., and McCormick, S.P. (2009). Genes, gene clusters, and biosynthesis of trichothecenes and fumonisins in *Fusarium*. Toxin Rev. **28:** 198–215.

Asran, M.R., and Eraky Amal, M.I. (2011). Aggressiveness of certain *Fusarium graminearum* isolates on wheat seedling and relation with their Trichothecence production. Plant Pathol. J. **10:** 36–41.

Boenisch, M.J., and Schäfer, W. (2011). *Fusarium graminearum* forms mycotoxin producing infection structures on wheat. BMC Plant Biol. **11:** 110.

Brecht, S., Carruthers, V.B., Ferguson, D.J.P., Giddings, O.K., Wang, G., Jäkle, U., Harper, J.M., Sibley, L.D., and Soldati, D. (2001). The toxoplasma micronemal protein MIC4 is an adhesin composed of six conserved apple domains. J. Biol. Chem. **276:** 4119–4127.

Bushnell, W.R., Hazen, B.E., and Pritsch, C. (2003). Histology and physiology of Fusarium head blight. In Fusarium Head Blight of Wheat and Barley, K.J. Leonard and W.R. Bushnell, eds (St. Paul, MN: APS Press), pp. 44–83.

Cai, S., and Lashbrook, C.C. (2006). Laser capture microdissection of plant cells from tape-transferred paraffin sections promotes recovery of structurally intact RNA for global gene profiling. Plant J. **48:** 628–637.

Catlett, N.L., Lee, B.N., Yoder, O.C., and Turgeon, B.G. (2003). Split-marker recombination for efficient targeted deletion of fungal genes. Fungal Genet. Newsl. **50:** 9–11.

Cook, R.J. (1968). Fusarium foot and root rot of cereals in the Pacific Northwest. Phytopathology **58:** 127–131.

Cuomo, C.A., et al. (2007). The *Fusarium graminearum* genome reveals a link between localized polymorphism and pathogen specialization. Science **317:** 1400–1402.

Dal Bello, G.M., Monaco, C.I., and Simon, M.R. (2002). Biological control of seedling blight of wheat caused by *Fusarium graminearum* with beneficial rhizosphere microorganisms. World J. Microb. Biot. **18:** 627–636.

Dash, S., Van Hemert, J., Hong, L., Wise, R.P., and Dickerson, J.A. (2012). PLEXdb: Gene expression resources for plants and plant pathogens. Nucleic Acids Res. **40**(Database issue)**:** D1194–D1201.

De Groot, P.W., Ram, A.F., and Klis, F.M. (2005). Features and functions of covalently linked proteins in fungal cell walls. Fungal Genet. Biol. **42:** 657–675.

DeZwaan, T.M., Carroll, A.M., Valent, B., and Sweigard, J.A. (1999). *Magnaporthe grisea* pth11p is a novel plasma membrane protein that mediates appressorium differentiation in response to inductive substrate cues. Plant Cell **11:** 2013–2030.

Divon, H.H., and Fluhr, R. (2007). Nutrition acquisition strategies during fungal infection of plants. FEMS Microbiol. Lett. **266:** 65–74.

Dufresne, M., van der Lee, T., Ben M'barek, S., Xu, X., Zhang, X., Liu, T., Waalwijk, C., Zhang, W., Kema, G.H., and Daboussi, M.J. (2008). Transposon-tagging identifies novel pathogenicity genes in *Fusarium graminearum*. Fungal Genet. Biol. **45:** 1552–1561.

Duplessis, S., et al. (2011). Obligate biotrophy features unraveled by the genomic analysis of rust fungi. Proc. Natl. Acad. Sci. USA **108:** 9166–9171.

Gaffoor, I., and Trail, F. (2006). Characterization of two polyketide synthase genes involved in zearalenone biosynthesis in *Gibberella zeae*. Appl. Environ. Microbiol. **72:** 1793–1799.

Güldener, U., Seong, K.Y., Boddu, J., Cho, S., Trail, F., Xu, J.R., Adam, G., Mewes, H.W., Muehlbauer, G.J., and Kistler, H.C. (2006). Development of a *Fusarium graminearum* Affymetrix GeneChip for profiling fungal gene expression in vitro and in planta. Fungal Genet. Biol. **43:** 316–325.

Harris, P.V., et al. (2010). Stimulation of lignocellulosic biomass hydrolysis by proteins of glycoside hydrolase family 61: Structure and function of a large, enigmatic family. Biochemistry **49:** 3305–3316.

Inoue, I., Namiki, F., and Tsuge, T. (2002). Plant colonization by the vascular wilt fungus *Fusarium oxysporum* requires *FOW1*, a gene encoding a mitochondrial protein. Plant Cell **14:** 1869–1883.

Jansen, C., von Wettstein, D., Schäfer, W., Kogel, K.H., Felk, A., and Maier, F.J. (2005). Infection patterns in barley and wheat spikes

inoculated with wild-type and trichodiene synthase gene disrupted *Fusarium graminearum*. Proc. Natl. Acad. Sci. USA **102:** 16892–16897.

Kazan, K., Gardiner, D.M., and Manners, J.M. (2012). On the trail of a cereal killer: Recent advances in *Fusarium graminearum* pathogenomics and host resistance. Mol. Plant Pathol. **13:** 399–413.

Kim, Y.T., Lee, Y.R., Jin, J., Han, K.H., Kim, H., Kim, J.C., Lee, T., Yun, S.H., and Lee, Y.W. (2005). Two different polyketide synthase genes are required for synthesis of zearalenone in *Gibberella zeae*. Mol. Microbiol. **58:** 1102–1113.

Kunze, M., Pracharoenwattana, I., Smith, S.M., and Hartig, A. (2006). A central role for the peroxisomal membrane in glyoxylate cycle function. Biochim. Biophys. Acta **1763:** 1441–1452.

Laluk, K., and Mengiste, T. (2010). Necrotroph attacks on plants: Wanton destruction or covert extortion? The Arabidopsis Book **8:** e0136, doi/10.1199/tab.0136.

Lamb, C., and Dixon, R.A. (1997). The oxidative burst in plant disease resistance. Annu. Rev. Plant Physiol. Plant Mol. Biol. **48:** 251–275.

Lorenz, M.C., and Fink, G.R. (2001). The glyoxylate cycle is required for fungal virulence. Nature **412:** 83–86.

Lysøe, E., Seong, K.Y., and Kistler, H.C. (2011). The transcriptome of *Fusarium graminearum* during the infection of wheat. Mol. Plant Microbe Interact. **24:** 995–1000.

Ma, L.J., et al. (2010). Comparative genomics reveals mobile pathogenicity chromosomes in *Fusarium*. Nature **464:** 367–373.

Malz, S., Grell, M.N., Thrane, C., Maier, F.J., Rosager, P., Felk, A., Albertsen, K.S., Salomon, S., Bohn, L., Schäfer, W., and Giese, H. (2005). Identification of a gene cluster responsible for the biosynthesis of aurofusarin in the *Fusarium graminearum* species complex. Fungal Genet. Biol. **42:** 420–433.

O'Donnell, K., Ward, T.J., Geiser, D.M., Corby Kistler, H., and Aoki, T. (2004). Genealogical concordance between the mating type locus and seven other nuclear genes supports formal recognition of nine phylogenetically distinct species within the *Fusarium graminearum* clade. Fungal Genet. Biol. **41:** 600–623.

Quinlan, R.J., et al. (2011). Insights into the oxidative degradation of cellulose by a copper metalloenzyme that exploits biomass components. Proc. Natl. Acad. Sci. USA **108:** 15079–15084.

Reid, L.M., Mather, D.E., Bolton, A.T., and Hamilton, R.I. (1994). Evidence for a gene for silk resistance to *Fusarium graminearum* Schw. ear rot of maize. J. Hered. **85:** 118–121.

Rittenour, W.R., and Harris, S.D. (2010). An in vitro method for the analysis of infection-related morphogenesis in *Fusarium graminearum*. Mol. Plant Pathol. **11:** 361–369.

Rocha, O., Ansari, K., and Doohan, F.M. (2005). Effects of trichothecene mycotoxins on eukaryotic cells: A review. Food Addit. Contam. **22:** 369–378.

Ruepp, A., Zollner, A., Maier, D., Albermann, K., Hani, J., Mokrejs, M., Tetko, I., Güldener, U., Mannhaupt, G., Münsterkötter, M., and Mewes, H.W. (2004). The FunCat, a functional annotation scheme for systematic classification of proteins from whole genomes. Nucleic Acids Res. **32:** 5539–5545.

Seong, K.Y., Zhao, X., Xu, J.R., Güldener, U., and Kistler, H.C. (2008). Conidial germination in the filamentous fungus *Fusarium graminearum*. Fungal Genet. Biol. **45:** 389–399.

Skibbe, D.S., Doehlemann, G., Fernandes, J., and Walbot, V. (2010). Maize tumors caused by *Ustilago maydis* require organ-specific genes in host and pathogen. Science **328:** 89–92.

Son, H., et al. (2011). A phenome-based functional analysis of transcription factors in the cereal head blight fungus, *Fusarium graminearum*. PLoS Pathog. **7:** e1002310.

Stephens, A.E., Gardiner, D.M., White, R.G., Munn, A.L., and Manners, J.M. (2008). Phases of infection and gene expression of *Fusarium graminearum* during crown rot disease of wheat. Mol. Plant Microbe Interact. **21:** 1571–1581.

Sturm, A., and Tang, G.Q. (1999). The sucrose-cleaving enzymes of plants are crucial for development, growth and carbon partitioning. Trends Plant Sci. **4:** 401–407.

Tang, W., Coughlan, S., Crane, E., Beatty, M., and Duvick, J. (2006). The application of laser microdissection to in planta gene expression profiling of the maize anthracnose stalk rot fungus *Colletotrichum graminicola*. Mol. Plant Microbe Interact. **19:** 1240–1250.

Tang, W.H., Zhang, Y., and Duvick, J. (2012). The application of laser microdissection to profiling fungal pathogen gene expression in planta. In Methods in Molecular Biology: Plant Fungal Pathogens, M. Bolton and B. Thomma, eds (Totowa, New Jersey: Humana Press), pp. 219–236.

Trail, F. (2009). For blighted waves of grain: *Fusarium graminearum* in the postgenomics era. Plant Physiol. **149:** 103–110.

Vogel, J. (2008). Unique aspects of the grass cell wall. Curr. Opin. Plant Biol. **11:** 301–307.

Walter, S., Nicholson, P., and Doohan, F.M. (2010). Action and reaction of host and pathogen during *Fusarium* head blight disease. New Phytol. **185:** 54–66.

Wang, C., et al. (2011). Functional analysis of the kinome of the wheat scab fungus *Fusarium graminearum*. PLoS Pathog. **7:** e1002460.

Wang, Z.Y., Thornton, C.R., Kershaw, M.J., Debao, L., and Talbot, N.J. (2003). The glyoxylate cycle is required for temporal regulation of virulence by the plant pathogenic fungus *Magnaporthe grisea*. Mol. Microbiol. **47:** 1601–1612.

Wolpert, T.J., Dunkle, L.D., and Ciuffetti, L.M. (2002). Host-selective toxins and avirulence determinants: What's in a name? Annu. Rev. Phytopathol. **40:** 251–285.

Wong, P., Walter, M., Lee, W., Mannhaupt, G., Münsterkötter, M., Mewes, H.W., Adam, G., and Güldener, U. (2011). FGDB: Revisiting the genome annotation of the plant pathogen *Fusarium graminearum*. Nucleic Acids Res. **39**(Database issue)**:** D637–D639.

Wu, A.B., Li, H.P., Zhao, C.S., and Liao, Y.C. (2005). Comparative pathogenicity of *Fusarium graminearum* isolates from China revealed by wheat coleoptile and floret inoculations. Mycopathologia **160:** 75–83.

Xu, J.R., Peng, Y.L., Dickman, M.B., and Sharon, A. (2006). The dawn of fungal pathogen genomics. Annu. Rev. Phytopathol. **44:** 337–366.

Yuan, T.L., Zhang, Y., Yu, X.J., Cao, X.Y., and Zhang, D. (2008). Optimization of transformation system of *Fusarium graminearum*. Plant Physiol. Commun. **44:** 251–256 (in Chinese).

In Planta Stage-Specific Fungal Gene Profiling Elucidates the Molecular Strategies of *Fusarium graminearum* Growing inside Wheat Coleoptiles

Xiao-Wei Zhang, Lei-Jie Jia, Yan Zhang, Gang Jiang, Xuan Li, Dong Zhang and Wei-Hua Tang

Plant Cell 2012;24;5159-5176; originally published online December 24, 2012;
DOI 10.1105/tpc.112.105957